Received 20 February 2024, accepted 13 March 2024, date of publication 27 March 2024, date of current version 2 April 2024.

Digital Object Identifier 10.1109/ACCESS.2024.3382134

RESEARCH ARTICLE

Voltage Feed-Forward Control of Photovoltaic-Battery DC Microgrid Based on Improved Seeker Optimization Algorithm

AIHUA WU[1], RUI GONG[1], JINGFENG MAO[1], XIUYONG YU[1], JIANJUN HE[2], AND E'XIANG LI[2]

[1]School of Mechanical Engineering, Nantong University, Nantong 226019, China
[2]Jiangsu Hantong Group, Nantong 226019, China

Corresponding author: Jingfeng Mao (mao.jf@ntu.edu.cn)

This work was supported in part by the Natural Science Research Program of Jiangsu Colleges and Universities under Grant 20KJA470002, and in part by the Excellent Teaching Team of ''Qinglan Project'' of Jiangsu Colleges and Universities.

ABSTRACT The photovoltaic-battery DC microgrid is a new type of power system supply architecture that can effectively utilize renewable energy and is suitable for modern DC electrical equipment. In this paper, a fast and efficient maximum power point tracking (MPPT) photovoltaic (PV) control method and a battery energy storage system (BESS) bus control method are proposed to improve the PV utilization and the bus voltage performance. Firstly, the principle of photovoltaic-battery and power balance is analyzed, and the mathematical model of each distributed generation in the DC microgrid is derived. Secondly, by introducing the voltage increment and time-varying smoothing factor, the exponential variable step perturbation and observation method for PV controller is proposed to accelerate the MPPT process. Considering the intermittent disturbance of PV energy absorption and large power fluctuation on the DC bus, parameters of BESS voltage controller are optimized by the improved seeker optimization algorithm (ISOA) which is improved by the variational Cauchy operator and chaotic initialization optimization strategy. Furthermore, to improve the voltage closed-loop response speed and reduce the hysteresis characteristics, a feed-forward compensation strategy is designed. Finally, multi-scheme simulation analyses are implemented in MATLAB/Simulink. Compared with the simulation results of traditional control method, the proposed method reduces the average voltage ripple percentage from 3% to 1% and improves the MPPT response speed from 70ms to 10ms. The simulation results verified the correctness and effectiveness of the proposed method.

INDEX TERMS DC microgrid, voltage stabilization control, PID control, seeker optimization algorithm, maximum power point tracking.

I. INTRODUCTION

The photovoltaic-battery DC microgrid is an applicable structure of renewable energy with high efficiency in absorbing PV energy and flexibility in meeting the DC demand. And it is receiving increasing attention [1], [2], [3]. In a photovoltaic-battery DC microgrid, the PV system and BESS are connected to the DC bus through a power electronic converter. To utilize more renewable energy, the PV system is often set up as the main power supply and the BESS as an auxiliary power supply, which maintains the power balance in the DC microgrid and suppresses fluctuations in the DC bus voltage by charging and discharging. Although DC microgrid do not need to consider the complex issues of reactive power, frequency fluctuation, phase synchronization, and tide current. The high-performance bus voltage control method is an important research point in photovoltaic-battery DC microgrid. Because there are highly non-linear characteristics of power electronic system, the complex intermittent characteristics of PV system, and the randomly changing load demand [4], [5], [6].

Traditional methods make it difficult to meet the power supply requirements of dynamic loads because they lack robustness to complex sunlight intensity and environmental

The associate editor coordinating the review of this manuscript and approving it for publication was Mauro Gaggero.

changes. Therefore, power management and non-linear control strategies need to be designed based on the output characteristics of each source and the dynamic mathematical model of the power electronic interface converter to ensure dynamic robust stability of the DC bus voltage. For example, reference [7] proposes a DC microgrid architecture for PV and BESS and designs an energy management strategy for optimal power flow to maintain the bus voltage and meet the load demand. Reference [8] proposes an isolated DC microgrid structure with PV, diesel generator, and BESS, and the energy management of all three is used to maintain the bus voltage stability. References [7] and [8] focus on the steady-state equations of each source and use the average energy model calculation to manage the output of each source to achieve power balance and voltage stability in the network.

Renewable energy has the characteristic of intermittent output, so the design of controllers is important. Reference [9] proposes a combined strategy of using gain scheduling method and centralized fuzzy logic control method for DC bus voltage control regulation to balance power dynamics and stabilize bus voltage. Although fuzzy control is easy to implement, further improvements are still needed in terms of logical rules and accuracy. Reference [10] proposed a model predictive voltage control strategy that uses a power linearization model to design closed-loop voltage control rules. The predictive controller based on linear models is limited to a limited operating range and accurate model parameter identification, which is insufficient in terms of adaptability to a wide operating range and robustness to suppress external uncertainties. Reference [11] proposes an Active Disturbance Rejection Control (ADRC) to control the charging and discharging of BESS and DC bus voltages. ADRC has the advantage of robustness in controlling model parameters and external disturbances, but its selection and control rules need to be optimized. Reference [12] proposes a nonlinear local state feedback controller that can effectively regulate voltage stability, but it is limited to constant load microgrids. Reference [13] proposes a PL-PI controller based on fuzzy logic for DC bus voltage control and regulation. But it has the problem of difficult parameter selection. Reference [14] proposes a controller designed based on backstepping method, which can effectively improve the robustness of the system, but has slight shortcomings in voltage balance and stability.

With the development of computational techniques, the introduction of parameter tuning into algorithms has proven to be a feasible and effective method. Genetic algorithms (GA) in [15], ant colony optimization (ACO) algorithms in [16], particle swarm optimization (PSO) algorithms in [17], and other algorithms are used to regulate the parameters of PID controllers. In the GA, the global search capability is strong enough to reach the sub-optimal solution quickly, but the local search capability is weak, and it often takes much time to reach the optimal solution. ACO is easy to deviate from the optimal solution if the parameters are not set properly due to its complex parameter setting. PSO is not effective in practical production because it tends to produce premature convergence and fall into local optimum solutions. Compared to the above multiple optimization algorithms, the seeker optimization algorithm (SOA) [18] has the advantages of simplicity of principle, fast convergence, and high search capability, but it still suffers from the disadvantages of slowing down the search speed at an early stage and the tendency to fall into a local optimum. To combat this problem, some scholars have proposed to introduce chaos theory into optimization algorithms [19]. The chaotic initialization is characterized by randomness, ergodicity, and regularity, which can effectively improve the solution accuracy and convergence performance of the algorithm.

This paper aims to design a high-performance control system with optimal parameter tuning function to improve control response speed, steady-state accuracy, and robustness under complex photovoltaic-battery work conditions. Proportional-integral-differential (PID) control method is one of the most practiced and reliable traditional control methods in the current industrial control environment. The PID controller has the advantages of strong stability, simple structure, easy implementation, robustness, and adaptability. It can monitor the controlled system states and adjust them with feedback in almost real-time. It also can conveniently regulate the control parameters according to different actual conditions to adapt to diverse environments and requirements. However, the control parameters are often poorly selected due to the complicated method of parameter turning, which leads to poor final performance in the production process. To improve the performance of the bus voltage of the photovoltaic-battery DC microgrid, this paper improves the SOA by introducing a chaotic initialization strategy and variational Cauchy operator. Using the improved SOA (ISOA), the parameters of the PID controller are optimized. By further adopting the feed-forward control strategy to suppress disturbances, it improves the DC bus voltage control response speed, accuracy, and the robustness.

In summary, the main contributions of this paper include: (1) The principle of photovoltaic-battery and power balance is analyzed, and the mathematical model of PV system and BESS in the DC microgrid is derived. (2) By introducing the PV voltage increment and time-varying smoothing factor, the MPPT PV controller with exponential variable step perturbation and observation method is developed to improve the operation efficiency. (3) Considering the intermittent disturbance of PV energy absorption and large power fluctuation on the DC bus, parameters of BESS voltage controller are optimized by the ISOA. (4) A DC bus voltage feed-forward controller is designed for BESS to realize the reasonable distribution of photovoltaic-battery power and the dynamic stabilization control of bus voltage. (5) The correctness and effectiveness of the proposed control method are verified by multi-scheme MATLAB/Simulink digital simulation.

The paper is organized as follows: Section II describes the working principle and mathematical modeling of photovoltaic-battery DC microgrid. In Section III, the MPPT controller for PV system and the ISOA-PID voltage controller for BESS are designed respectively. In Section IV, four simulation schemes, as well as three operation conditions are designed, and the correctness and effectiveness of the control method proposed in this paper are verified by the simulation comparison results. Finally, the research conclusions and future research trends of this paper are described in Section V.

II. WORKING PRINCIPLE AND MATHEMATICAL MODELING OF PHOTOVOLTAIC-BATTERY DC MICROGRID

A. STRUCTURE OF PHOTOVOLTAIC-BATTERY DC MICROGRID

Fig.1 shows the overall structure of the photovoltaic-battery DC microgrid, including components such as the PV system, the BESS, and the DC load. P_{pv}, P_{bess}, P_{load}, and P_{net} are the PV output power, BESS output power, load power, and total bus power, respectively. V_{dc} and C_{dc} are the bus voltage and bus equivalent capacitance, respectively.

To maximize the utilization of renewable energy, the PV system is configured as a power main supply, connected to the common DC bus via a DC-DC boost converter. The BESS is an energy storage and stabilization power supply, connected to the DC bus via a bi-directional DC-DC converter. The BESS stores excess energy generating from the PV system under strong sunlight conditions and releases energy to DC microgrid under heavy load conditions. It maintains bus voltage dynamic stability through fast charge and discharge control.

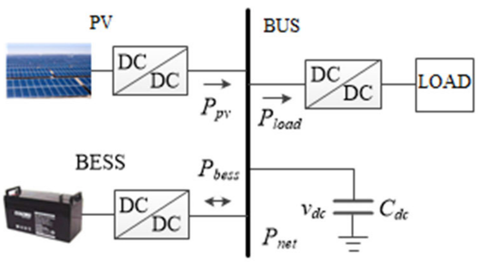

FIGURE 1. Typical structure of DC microgrid system.

B. PRINCIPLE OF DC BUS POWER BALANCING

According to the power conservation principle, the total power P_{net} balance equation of the photovoltaic-battery DC microgrid can be expressed as

$$P_{net} = P_{pv} + P_{bess} - P_{load} \tag{1}$$

The PV system operates in MPPT power generation mode and outputs positive power to the microgrid. The BESS output power is negative in charging mode and positive in discharging mode. For all operating conditions, ensuring constant DC bus voltage is the primary task to ensure stable operation of the microgrid. Therefore, under steady-state constant voltage conditions, the input-output power on the bus remains zero, i.e. $P_{net} = 0$. Under dynamic conditions, the relationship between power and voltage can be expressed as:

$$v_{dc}\frac{dv_{dc}}{dt} = \frac{1}{C_{dc}}P_{net} \tag{2}$$

Thus, it is necessary to control the charging and discharging of the BESS based on the power fluctuations to ensure the stability of the DC bus voltage.

C. MATHEMATICAL MODEL OF THE PV SYSTEM

Usually, the PV system consists of many individual PV cells connected in series and parallel. These PV cells form a PV array and use a DC-DC boost converter to match the output voltage of the PV array with the DC microgrid common bus voltage [20]. The equivalent circuit of a PV system is shown in Fig.2.

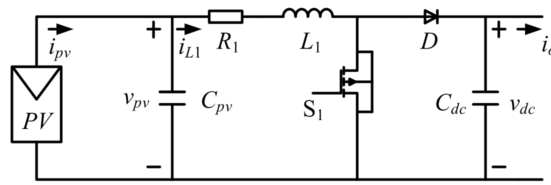

FIGURE 2. Equivalent circuit of the PV system.

In Fig 2, V_{pv}, C_{pv}, and i_{pv} are the PV array output voltage, filter capacitor, and output current, respectively. R_1, D, L_1, and i_{L1} are the boost converter resistor, diode, inductor, and inductor current, respectively. i_{o1} is the DC system equivalent load current.

The duty cycle control quantity of the power electronic switch S_1 is μ_1, then according to Kirchhoff's circuit rule, the mathematical model of the PV system shown in Fig.2 can be expressed as [21].

$$\begin{cases} \dot{v}_{pv} = \dfrac{1}{C_{pv}}\left(i_{pv} - i_{L1}\right) \\ \dot{i}_{L1} = \dfrac{1}{L_1}\left(-R_1 i_{L1} + v_{pv} - (1-\mu_1)\, v_{dc}\right) \\ \dot{v}_{dc} = \dfrac{1}{C_{dc}}\left(1-\mu_1\right) i_{L1} - \dfrac{1}{C_{dc}} i_{o1} \end{cases} \tag{3}$$

The PV array is connected to the DC bus via a DC-DC boost converter. Due to the intermittent nature of solar power, the MPPT method is often used to control the boost converter so that the output of the PV system is a Constant Power Source (CPS).

D. MATHEMATICAL MODEL OF THE BESS

The BESS consists of a battery bank and a bi-directional DC-DC converter, the equivalent circuit of which is shown in Fig.3.

In Fig.3, V_g and C_g are the BESS battery bank output terminal voltage and filter capacitance, respectively. L_2, R_{L2}, and i_{L2} are the inductor, inductor parasitic resistance, and inductor current of the bi-directional DC-DC converter, respectively. i_d is the current flowing through the power electronic

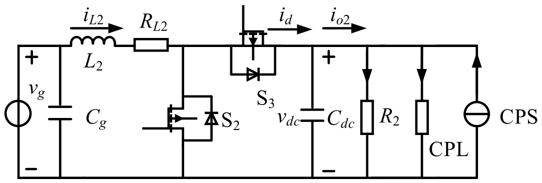

FIGURE 3. Equivalent circuit of the BESS.

switch S_3. i_{o2} is the DC system equivalent load current. R_2 is the resistive load. P_{CPL} is the constant power load power. And i_{CPS} is the CPS output current.

The duty cycle control quantity of the power electronic switch S_2 is μ_2, then according to Kirchhoff's circuit rule, the mathematical model of the BESS shown in Fig.3 can be expressed as [22].

$$\begin{cases} C_{dc}\dfrac{dv_{dc}}{dt} = \mu_2 i_{L2} - i_{o2} \\ i_{o2} = \dfrac{v_{dc}}{R_2} + \dfrac{P_{CPL}}{v_{dc}} - i_{CPS} \\ v_g i_{L2} = v_{dc} i_d \end{cases} \tag{4}$$

S2 and S3 operate in complementary conduction mode, the inductor current dynamic equation can be expressed as

$$L_2\frac{di_{L2}}{dt} = v_g + \mu_2 v_{dc} + R_{L2} i_{L2} \tag{5}$$

When S_3 is conducting, the converter works in buck mode and the BESS is charging. When S_2 is conducting, the converter works in boost mode and the BESS is discharging. The BESS charging or discharging is controlled by adjusting PWM duty cycle of the power electronic switch to maintain DC bus voltage stability.

III. OPTIMAL DESIGN OF CONTROL METHODS

In DC microgrid, the individual distributed source parameters are time-varying and non-linear, and the operating conditions is complex, which makes it difficult to maintain a long-term steady state. So robust and stable operation control of DC microgrid is important.

Traditional PID control is a popular linear control method, but its controller design is based on a model that adopts approximate linearization treatment near the system equilibrium point, and the actual control effect is not good. This paper adopts variable step perturbation and observation method MPPT control to improve the operating efficiency of PV system according to the principle of maximum renewable energy utilization, and uses ISOA-PID control for BESS to obtain a good voltage robust control effect.

A. DESIGN OF MPPT CONTROLLER FOR THE PV SYSTEM

The PV cells' output characteristics refer to the relationship between the output power and output voltage, which is shown in Fig.4. The PV cell's V-I characteristics are non-linear. In most of the working voltage range, the output current is constant and is comparable to the short-circuit current. But when the output voltage is close to the open circuit voltage, the current drops very quickly, making the output power characteristics as a single-peak function with a maximum power point (MPP).

PV cells should work at the MPP as much as possible to increase the efficiency of the PV system. However, the sunlight intensity and temperature are constantly changing in practice. The principle of maximum power point tracking is to adjust the equivalent input impedance through certain control devices and strategies, so that the PV cells can obtain the maximum possible output power. In fact, it is an autonomous optimization process [23], [24].

The MPPT perturbation and observation method is simple and easy to implement. However, it is influenced by the perturbation step size so much that it cannot adapt to the changing environment. The voltage tends to oscillate when the perturbation step size is too large, and the tracking speed is slow when the perturbation step size is too small. The exponentially variable step method makes the step size larger when it is far from the MPP and smaller when it is close to the MPP. By combining the perturbation and observation method with an exponentially variable step method, MPPT can be achieved with excellent tracking speed and accuracy. In this paper, MPPT control is based on the power variation exponential variable step perturbation and observation method, which is achieved by adjusting the duty cycle μ_1.

The proposed exponential variable step perturbation and observation method introduces a time-varying smoothing factor m for the voltage increment ΔU in the traditional fixed-step perturbation and observation method. The value of m is between (0,1), and it is related to the distance from the MPP. When the distance to the MMP is far, m takes on a large value. Conversely, m takes on a small value. This makes the step size ΔU no longer a constant value, but a function related to the time-varying coefficient m [25].

As shown in Fig.4, the slope of the P-U characteristic curve is larger, and the ΔP increment is larger as the operating point moves away from the MPP. The slope becomes smaller, and the ΔP increment is smaller as the operating point approaches the MPP. The magnitude of the value of m is changed depending on the variation of ΔP. The m takes on a large value when ΔP is large, which near close to 1. When ΔP is small, m takes on a small value. ΔP is mapped directly to the value of m through the exponential function. The m takes on a value that

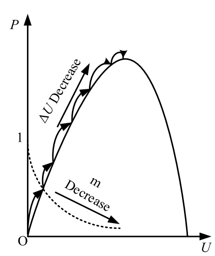

FIGURE 4. Schematic diagram of MPPT step change.

changes in real-time as ΔP changes, and the expression is

$$m = 1 - \exp\left(-\|\Delta P\|^2\right) \tag{6}$$

The specific flow of the proposed exponential variable step perturbation and observation method control is shown in Fig.5. At the beginning, the method measures the U and I at the current operating point and calculates the value of ΔP and ΔU from the previous operating point. Then it obtains the value of the time-varying factor m from the exponential function operation to decide the step size at the next operating point. By comparing the positive and negative values of $\Delta P \Delta U$, the direction of disturbance of the given voltage reference at the next operating point, and the voltage reference value $U_{ref}^{*} = U_{ref} \pm m\Delta U$ are finally obtained for the next operating point.

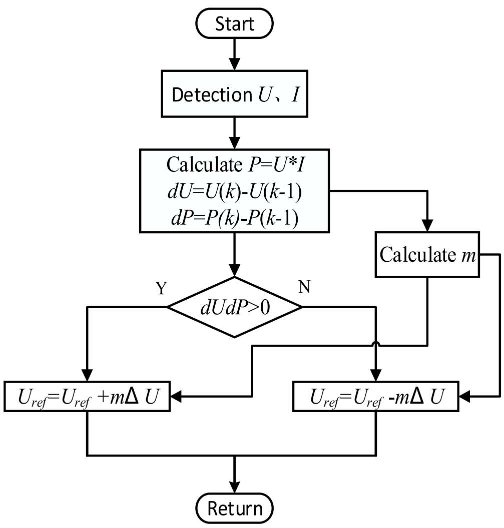

FIGURE 5. Flow of the proposed exponential variable step perturbation and observation method control.

B. DESIGN OF THE ISOA-PID VOLTAGE CONTROLLER FOR THE BESS

PID controllers are widely used in the field of DC microgrid control, and in order to achieve better control effects, PID parameter optimization is a hot research topic. It is of great significance for the stability, reliability, and fast response characteristics of the BESS control system. In this paper, the seeker optimization algorithm (SOA) is proposed to improve and optimize the performance of PID controllers. The PID parameters are set as the search target, and the absolute value of the error and the time integral of the squared control input term as the optimization target. Then the optimal control quantity of the system is obtained after iterative search and calculation.

1) THE SOA PRINCIPLES ANALYSIS

SOA is a new type of intelligent algorithm for human population behavior. It treats the set sum of search behaviors as the initial population, and the behavior individuals as individual solutions. The algorithm's inference judgment of position and direction are achieved by simulating human search patterns, and ultimately the optimal solution to the problem can be obtained [26].

a: SELECTION OF THE FITNESS FUNCTION

This paper uses the error absolute integral value to construct the minimum objective function to expect a suitable dynamic iterative property to guide the algorithm to optimize in the direction of the control objective. The constructed minimum objective function f is defined as

$$f = \begin{cases} \int_0^{\infty} \left[\eta_1 |e(k)| + \eta_2 u^2(k)\right] dk, & e(k) \geq 0 \\ \int_0^{\infty} \left[\eta_1 |e(k)| + \eta_2 u^2(k) + \eta_3 |e(k)|\right] dk, & e(k) < 0 \end{cases} \tag{7}$$

where η_1, η_2, and η_3 are weights; $e(k)$ is the system error; $u(k)$ is the control input. To meet the optimization requirements and reduce the system error, making $\eta_1 > \eta_2$, $\eta_1 + \eta_2 = 1$. Usually, the penalty mechanism is used, where $\eta_1 = 0.999$, $\eta_2 = 0.001$, and $\eta_3 = 100$, to avoid overshoot.

b: DETERMINATION OF EXPLORATION STEP SIZE

SOA follows the seeker rules and uses the approximation function of the fuzzy system with a Gaussian subordination function to represent the search step fuzzy variables.

$$u_A(x) = e^{-(x-u)^2/2\delta^2} \tag{8}$$

where u_A is the Gaussian affiliation; x is the input variable; u and δ are the parameters of the affiliation function. Using the linear affiliation function, the best position corresponds to the maximum affiliation value $u_{max} = 1.0$. Since the affiliation is less than 0.0111 when the input exceeds [u-3δ, $u+3\delta$], it can be ignored, i.e., the worst position corresponds to the smallest affiliation $u_{min} = 0.0111$, and the other positions correspond to 0.0111< u <1. The Gaussian distribution as Fig.6.

$$u_{i,j} = rand\,(u_i, 1)\; (j = 1, 2, \cdots, D) \tag{9}$$

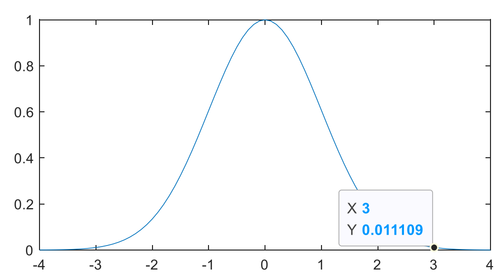

FIGURE 6. Gaussian distribution.

where u_i is the affiliation of the objective function value i; $u_{i,j}$ is the affiliation of the objective function value i in the j-dimensional search space; D is the dimension of the search space. Because the optimization objective is the three parameters of the PID, $D = 3$.

The search step $a_{i,j}$ is given by

$$\alpha_{i,j} = \delta_{i,j}\sqrt{-\ln\left(u_{i,j}\right)} \tag{10}$$

where $\delta_{i,j}$ is the parameters of the Gaussian affiliation function; $u_{i,j}$ is the affiliation degrees of the search space objective function. Its value is obtained by the following equations

$$\delta_{i,j} = \eta_0 \times |x_{\max} - x_{\min}| \tag{11}$$

$$\eta_0 = (T - t)/T \tag{12}$$

where η_0 is the inertia weight; x_{max} and x_{min} are the positions of the population's maximum and minimum function values; T and t are the maximum number of iterations and the current number of iterations, respectively.

c: DETERMINATION OF SEARCH DIRECTION

Analytical modeling of the egoist direction defined as d_e, the altruistic direction defined as d_a, and the proactive direction defined as d_p. They can be expressed as

$$\begin{cases} \vec{d}_e(t) = \vec{p}_{best} - \vec{x}(t) \\ \vec{d}_a(t) = \vec{g}_{best} - \vec{x}(t) \\ \vec{d}_p(t) = \vec{x}(t_1) - \vec{x}(t_2) \end{cases} \tag{13}$$

where p_{best} is the optimal position in individual history; g_{best} is the global historical optimal location; $x(t_1)$ and $x(t_2)$ are the optimal positions in $\{x(t\text{-}2), x(t\text{-}1), x(t)\}$, respectively.

The search direction d_f is determined using a random weighted geometric average of the three directions which can be expressed as

$$d_f(t) = sign(\eta_0 d_p + m_1 d_e + m_2 d_a) \tag{14}$$

where $sign()$ is the sign function; m_1 *and* m_2 are real numbers in the interval [0-1].

d: UPDATE OF INDIVIDUAL LOCATIONS

After getting the search step $a_{i,j}$ and the search direction d_f, the individual position update is carried out. The updated position $x_{i,j}(t+1)$ can be expressed as

$$x_{ij}(t+1) = x_{ij}(t) + \alpha_{ij}(t)\, d_f(t) \tag{15}$$

2) ISOA ALGORITHM

In order to solve the problem of low search efficiency in the early stage and the inability to find the global optimal solution due to local extremum in the later stage of the SOA algorithm [27], ISOA based on the chaotic initialization optimization strategy and the Cauchy variational operator is proposed.

Compared with Square, Sine, and other mappings, Logistic chaos mapping has the best performance, and can generate more symmetric and uniform random number distributions [28], [29]. Therefore, in this paper, Logistic chaos mapping function is chosen to iterate population.

$$x(\Phi + 1) = \mu x(\Phi)\left[1 - x(\Phi)\right] \tag{16}$$

where Φ is the number of iterations; μ is the regulation parameter ($0<\mu<1$).

There generates a random D-dimensional benchmark particle y_0, in the interval (0,1), $y_0 = (y_{01}, y_{02}, y_{03}, \ldots, y_{0H})$, then, the set of chaotic populations $y_{n+1,j}$ can be expressed as

$$y_{n+1,j} = \mu y_{n,j}(1 - y_{n,j}) \tag{17}$$

Next, map (0,1) into the search space [-Γ, Γ] to obtain the D-dimensional particle population $x_{n+1,j}$ which can be expressed as

$$x_{n+1,j} = \Gamma \times (2 \times y_{n+1,j} - 1) \tag{18}$$

where $n = 0,1,2,\ldots,N$, $j = 1,2,\ldots, D$; N is the population size and D is the search space dimension, there, $N = 20$ and $D = 3$.

The initial positions of the particle swarm obtained by the logistic chaotic mapping function can effectively improve the pre-search efficiency compared with the initial positions obtained by pseudo-random numbers.

The Cauchy variational operator is introduced to solve the phenomenon of falling into local extrema in the late stage of the search. The performance of the Cauchy distribution is like that of the Gaussian distribution, as shown in Fig. 7. The main difference is that the Cauchy distribution function has longer wings, and its generated random numbers have a wider range of variances. So, the ability to jump out of the local optimal solution in the process of algorithm position update becomes stronger. The formula for the Cauchy variation is [30] and [31]

$$A(t) = \begin{cases} x_{i,j}^t \times cauchy\,(0,1)\,,\ rand\,(0,1) \le p \\ x_{i,j}^t,\ rand\,(0,1) > p \end{cases} \tag{19}$$

where p is the random rate of variation; *Cauchy* (0,1) is the standard Cauchy distribution function.

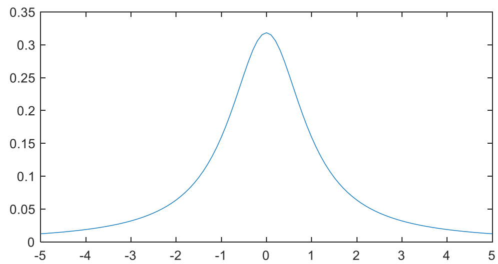

FIGURE 7. Cauchy distribution.

Then, using the Cauchy distribution to perform a mutation operation on g_{best} as

$$\begin{cases} g_{best,j}^{t+1} = g_{best,j}^{t} + \gamma \times A(t) \\ \gamma = e^{-\frac{\lambda t}{T}} \end{cases} \tag{20}$$

where γ is the mutation weight; g_{bestj} is the global optimal j dimensional component; λ is chosen as a constant, λ = 10; T is the maximum number of iterations and t is the current number of iterations.

3) DESIGN OF FEED-FORWARD CONTROLLER BASED ON ISOA

Considering the delay problem in the feed-back control process of traditional PID control, which can cause control delay or even failure, a feed-forward compensation PID control method is proposed. The purpose is to reduce the system tracking error by compensating PID with feed-forward compensation. It can also ensure the fast response of the system, improve the tracking accuracy of the controller and the control accuracy of the system. The principal block diagram is shown in Fig.8.

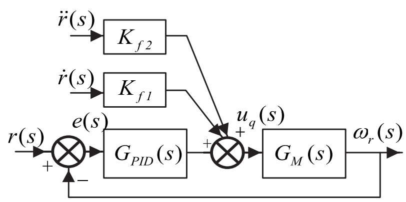

FIGURE 8. **Block Diagram of Feed-forward PID Controller.**

The system transfer function $\omega_r(s)/r(s)$ and the system error transfer function $e(s)/r(s)$ can be expressed as

$$\begin{cases} \dfrac{\omega_r(s)}{r(s)} = \dfrac{\left[G_{PID}(s) + K_{f1}\dot{r}(s) + K_{f2}\ddot{r}(s)\right] G_M(s)}{1 + G_{PID}(s)G_M(s)} \\ \dfrac{e(s)}{r(s)} = 1 - \dfrac{\left[G_{PID}(s) + K_{f1}\dot{r}(s) + K_{f2}\ddot{r}(s)\right] G_M(s)}{1 + G_{PID}(s)G_M(s)} \\ = \dfrac{1 - \left[K_{f1}\dot{r}(s) + K_{f2}\ddot{r}(s)\right] G_M(s)}{1 + G_{PID}(s)G_M(s)} \end{cases} \tag{21}$$

where r(s) is the initial input signal; uq(s) is the voltage input under the Rasch transform; GPID(s) is the PID transfer function under the Rasch transform; e(s) is the speed tracking error under the Rasch transform; Kf1 and Kf2 are both feed-forward gain coefficients.

When $K_{f_1}\dot{r}(s) + K_{f_2}\ddot{r}(s) = 1/G_M(s)$, the system error can be theoretically eliminated. Although the system error cannot be eliminated in practice, it can be reduced to an acceptable level. The robust control stability of the photovoltaic-battery DC microgrid is greatly improved without affecting the system stability as much as possible.

For cases where the PID sampling period Tc is short, the continuous system can be converted directly into a discrete system by PID discretization processing. Therefore, the feed-forward compensated PID discrete control law can be expressed as

$$u_q(k) = K_p e(k) + K_i \sum_{l=0}^{k} e(l) + K_d\left(e(k) - e(k-1)\right) + K_{f1}\dot{r}(k) + K_{f2}\ddot{r}(k) \tag{22}$$

For a photovoltaic-battery DC microgrid system with non-linearity and hysteresis, it is difficult to adjust the parameters of a PID controller with a simple structure and easy implementation. Therefore, PID parameters self-tuning based on ISOA is used to achieve global optimal control of the system.

4) ISOA-PID CONTROL PRINCIPLE

Using the feed-forward compensation PID control method based on the ISOA, the output speed tracking value and its error value are optimized and processed separately. And the three parameters K_p, K_i, and K_d of the controller are adjusted to improve speed tracking accuracy and eliminate speed tracking errors. The control system principle is shown in Fig.9.

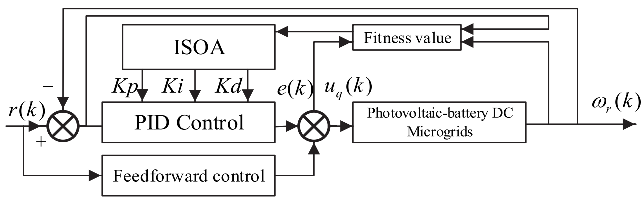

FIGURE 9. **Principal diagram of control system.**

The flow of the ISOA-PID control method is as follows: ① Initialize the population and parameters with chaos. ② Update the velocity and position of each particle. ③ Evaluate the fitness value of each particle and update the local and global optimal position. ④ Perform global optimal Cauchy variation operation. ⑤ Compare the population history optimal position with the current individual optimal position, and update and replace the population history optimal position

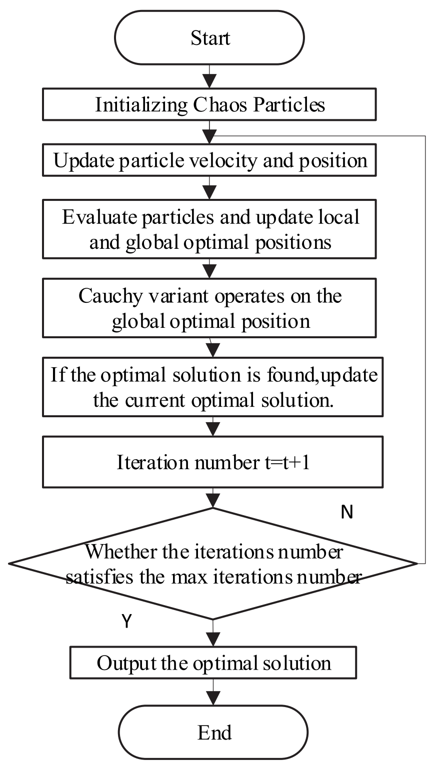

FIGURE 10. **ISOA-PID flow chart.**

if the current individual optimal position is better. ⑥ If the termination condition is satisfied, output the optimal value and optimal solution, otherwise, return to step ②. The flow chart of ISOA-PID is shown in Fig.10.

IV. SIMULATION VERIFICATION AND ANALYSIS

To verify the effectiveness and correctness of the proposed control method for photovoltaic-battery DC microgrid, MATLAB / Simulink is used for simulation research. The system parameters are shown in Table 1.

TABLE 1. Circuit parameters of photovoltaic-battery DC microgrid.

PV system parameters	Numerical values	*BESS* module parameters	Numerical values
Maximum power	10kW	Battery capacity	100Ah
Open-circuit voltage	37.2V	Open circuit voltage	300V
Short-circuit current	8.62A	C_g for standard values	1μF
Max. power voltage	30.2V	R_{L2} for standard values	100Ω
Maximum power current	8.1A	Standard values for L_2	0.01H
C_{pv} standard values	10μF		
L_{pv} Standard values	5mH		
R_{pv} standard values	0.005Ω		
C_{dc} standard values	1μF		

A. CONTROL VALIDATION OF THE PV SYSTEM EXPONENTIAL VARIABLE STEP PERTURBATION AND OBSERVATION METHOD

A real PV system consists of several PV cells, and its maximum power is calculated by adding up the maximum power of all PV cells. The maximum power of commonly used PV cells in the market currently ranges from 200W to 300W. To simulate real situations as much as possible, in this paper, the PV system consists of 50 PV cells, each with a maximum power of 200W under sunlight intensity of 1600 m^2/W on 25°C. To facilitate the establishment of a simulation model, one PV cell was selected for MPPT simulation in the PV system.

Set the initial sunlight intensity to 1400m^2/W and the temperature to 25°C. In this condition, the theoretical MPP is 177.77W. Set the step size of traditional disturbance observation to 0.1V. The simulation waveform diagram of the exponential variable step perturbation and observation method and the traditional disturbance observation method of the PV MPPT control are shown in Fig.11.

As shown in Fig. 11 (a), the exponential variable step disturbance observation method reaches stability in 10ms. The traditional disturbance observation method reaches stability in 70ms. As shown in Fig. 11 (b), the output power of

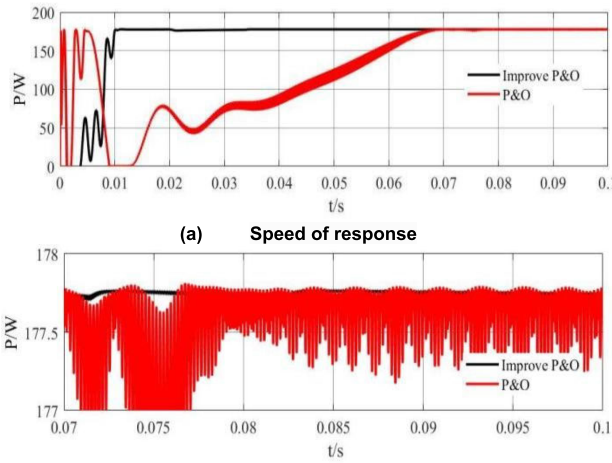

(a) Speed of response

(b) Steady-state output power

FIGURE 11. Simulation comparison diagram.

TABLE 2. Comparison of MPPT control result with different methods.

Method	Speed of response	ripple value ((W_{max}–W_{min})/$W_{theoretical}$)
exponential variable step perturbation and observation	10ms	0.07‰
traditional disturbance and observation method	70ms	2.81‰

the exponential variable step disturbance observation method remains stable within the range of 177.757W-177.77W, with amplitude fluctuations of around 0.013W. Compared with the theoretical value, its ripple is 0.07 ‰. The amplitude fluctuation of traditional disturbance observation method is 0.5W. Compared with the theoretical value, its ripple is 2.81 ‰. The propose method energy loss of the PV system is small, and it has high steady-state stability. It has better stability and rapidity for the MPPT control of the PV system.

The ambient temperature is set to remain constant at T = 25°C. The sunlight intensity is 1000W/m^2, 900W/m2, 800W/m^2, and each phase is maintained for 0.2s, and then returned to 1000W/m^2. The MPPT simulation waveform of the PV system with exponential variable step perturbation and observation method is shown in Fig.12.

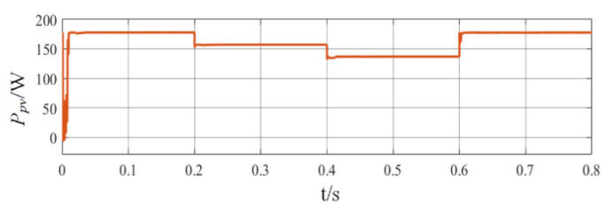

FIGURE 12. MPPT simulation of constant temperature and variable sunlight intensity.

As shown in Fig.12, the response speed, steady-state stability, and dynamic transition process of the proposed MPPT control method are excellent when the ambient temperature remains constant at T = 25°C and the sunlight intensity changes at 0.2s, 0.4s, and 0.6s, respectively.

B. VERIFICATION OF ISOA-PID CONTROL FOR BESS

The preferred parameters in the ISOA-PID controller are: $\Phi = 100$, $\eta_1 = 0.999$, $\eta_2 = 0.001$, $\eta_3 = 100$, $_1 = 0.7$ and $m_2 = 0.45$.

The preferred parameters in the traditional PID controller are: $K_p = 0.03$, $K_i = 0.001$, $K_d = 0.0002$ [32].

1) CONDITION 1: CONSTANT SUNLIGHT INTENSITY AND LOAD DEMAND

First, the PV system is set to operates under standard atmospheric conditions, with an initial sunlight intensity of 1000 W/m^2, a temperature of 25°C, and a rated bus V_{dc} = 600 V. Under this condition, it is assumed that the sunlight intensity and load demand are constant, and the output power of the PV system is lower than the load. The DC-DC converter of the PV system and the bi-directional DC-DC converter of the BESS are required to jointly output power to meet the load demand.

At the initial moment of the simulation, the load consumption is constant at P_{CPL} = 3kW and i_{CPL} = 5A according to Ohm's law. Fig.13(a)-(e) show the DC bus voltage, PV output power, load power consumption, BESS power input, and load current waveforms, respectively.

As shown in Fig.13(a), the bus voltage of the DC microgrid is stable. The PID-controlled bus voltage shows oscillation, with the highest value of 611 V, and the lowest value of 592 V. The highest oscillation point of the ISOA-PID-controlled bus voltage is 606 V, and the lowest oscillation point is 597 V. This shows that the ISOA-PID is more stable and has less oscillation than the PID.

As shown in Fig.13(b), the PV system reaches a steady state at 0.2s. The MPPT control algorithm calculates that the maximum output power is maintained at around 5kW, i.e., P_{pv} = 5kW. The PV system output power is not affected by the DC microgrid, but only by the sunlight radiation level and temperature.

As shown in Fig.13(c), the load power consumption reaches a steady state at 0.2s with a constant P_{CPL} = 3kW, indicating that the load power of the DC microgrid system reaches balance with P_{load} = 3kW.

As shown in Fig.13(d), the ISOA-PID controlled the power waveform of the BESS. The BESS acts as a power source to maintain the bus voltage and is used to absorb the excess power from the PV system. The BESS reaches a steady state at 0.2s. The BESS input power is maintained at around 2kW and $P_{bess} = -2$kW. The load power consumption is equal to the sum of the PV power consumption and the power absorbed by the BESS. According to equation (1), the net grid power P_{net} = 0W, the bus voltage is stable and achieves the desired result.

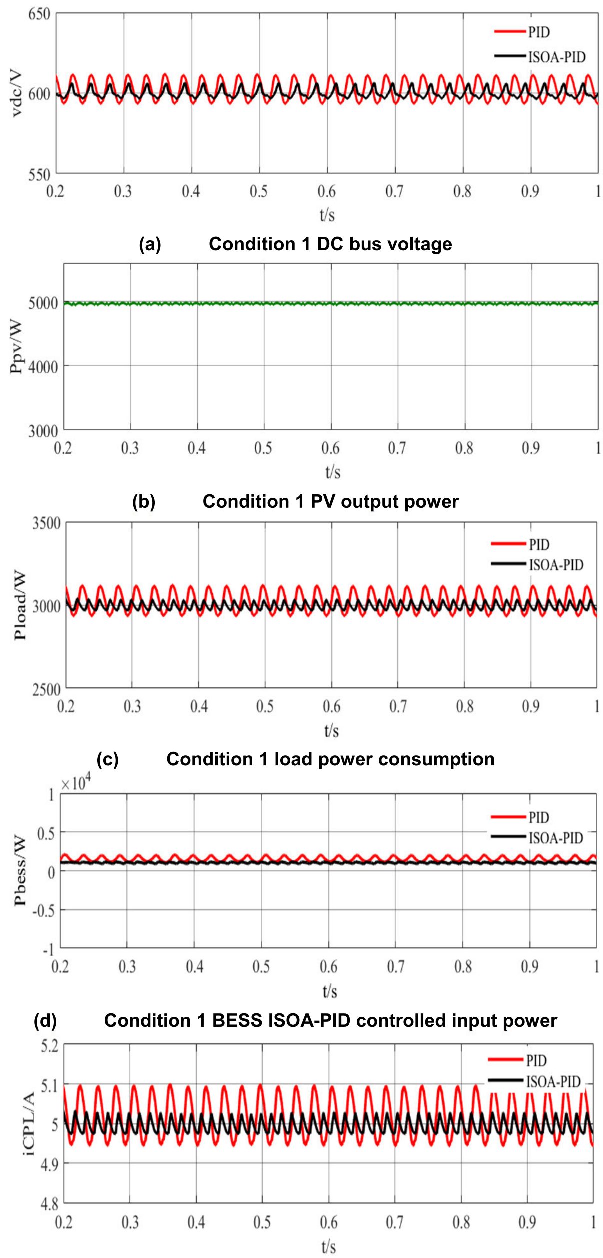

(a) Condition 1 DC bus voltage

(b) Condition 1 PV output power

(c) Condition 1 load power consumption

(d) Condition 1 BESS ISOA-PID controlled input power

(e) Condition 1 load current

FIGURE 13. Output characteristics of microgrid under condition 1.

As shown in Fig. 13(e), after the load current reaches the steady state at 0.2s, the highest fluctuation value of PID control i_{CPL} = 5.1A, and the lowest fluctuation value i_{CPL} = 4.95A. The highest fluctuation value of ISOA-PID control is i_{CPL} = 5.03A, and the lowest fluctuation value is i_{CPL} = 4.97A, which is stable at about 5A. It is consistent with the theoretical operation results from the simulation results.

The data from the above simulation results are shown in Table 3. The proposed ISOA-PID control method is superior to the traditional PID control method in stabilizing bus voltage oscillations and suppressing load current fluctuations under constant conditions.

TABLE 3. Stability performance of two control methods under condition 1.

Control method	Bus voltage			Load current
	Highest oscillation value	Lowest oscillation value	ripple percentage ((*Vmax–Vmin)/Vavg*)	ripple percentage ((*Imax–Imin)/Iavg*)
PID	611V	592V	3.2%	3.0%
ISOA-PID	606V	597V	1.5%	1.2%

2) CONDITION 2: CONSTANT SUNLIGHT INTENSITY WITH VARYING LOAD POWER

The condition is set to constant sunlight intensity, varying load power, and the PV system output power lower than the load. Under this condition, the DC-DC converter of the PV system and the bi-directional DC-DC converter of the BESS are required to jointly output power to meet the load demand.

At the initial moment of the simulation, the load consumption is constant at $P_{CPL} = 3$kW. The load consumption is constant at $P_{CPL} = 8$kW after 0.5s. According to Ohm's law, the load current $i_{CPL} = 5$A before 0.5s and $i_{CPL} = 13.33$A after 0.5s.

Fig.14 shows the simulation waveforms of DC bus voltage, load power consumption, BESS power input, and load current respectively.

As shown in Fig.14(a), the bus voltage of the PID DC microgrid is stable. The highest oscillation value before 0.5s is 619V, and the lowest oscillation value is 599V. After 0.5s, the highest oscillation value is 604V, and the lowest oscillation value is 583V. But about the ISOA-PID, the highest oscillation value before 0.5s is 602V. The lowest oscillation value is 599V. After 0.5s, the highest oscillation value is 604V, and the lowest oscillation value is 595V. This indicates that ISOA-PID is more stable than PID and has a better control effect.

As shown in Fig.14(b), the power load reaches a steady state at 0.2s, with a constant load consumption of $P_{CPL} = 3$kW before 0.5s and a constant $P_{CPL} = 8$kW after 0.5s, $P_{load} = 3$kW before 0.5s and maintained at $P_{load} = 8$kW after 0.5s, indicating that the total power of the DC microgrid system is balanced.

As shown in Fig.14(c), the BESS power is used to maintain the bus voltage stable and to absorb or compensate for the lack or excess power of the PV system. The BESS reaches the steady state at 0.2s, the input power is maintained at around 2kW before 0.5s, i.e., $P_{bess} = -2$kW, and the output power is maintained at around 3kW after 0.5s, i.e., $P_{bess} = 3$kW. The dynamic transition time is about 0.02s, and the output power is quickly switched. The load power consumption is equal to the sum of the PV output power and the power provided by the BESS. According to equation (1), the net grid power $P_{net} = 0$W, the bus voltage is stable, and the desired result is obtained.

As shown in Fig.14(d), after the load current reaches the steady state at 0.2s, the load current i_{CPL} is 5A before 0.5s. The load current i_{CPL} is 13.3A after 0.5s. ISOA-PID control is more stable than PID control, and the load current fluctuates less.

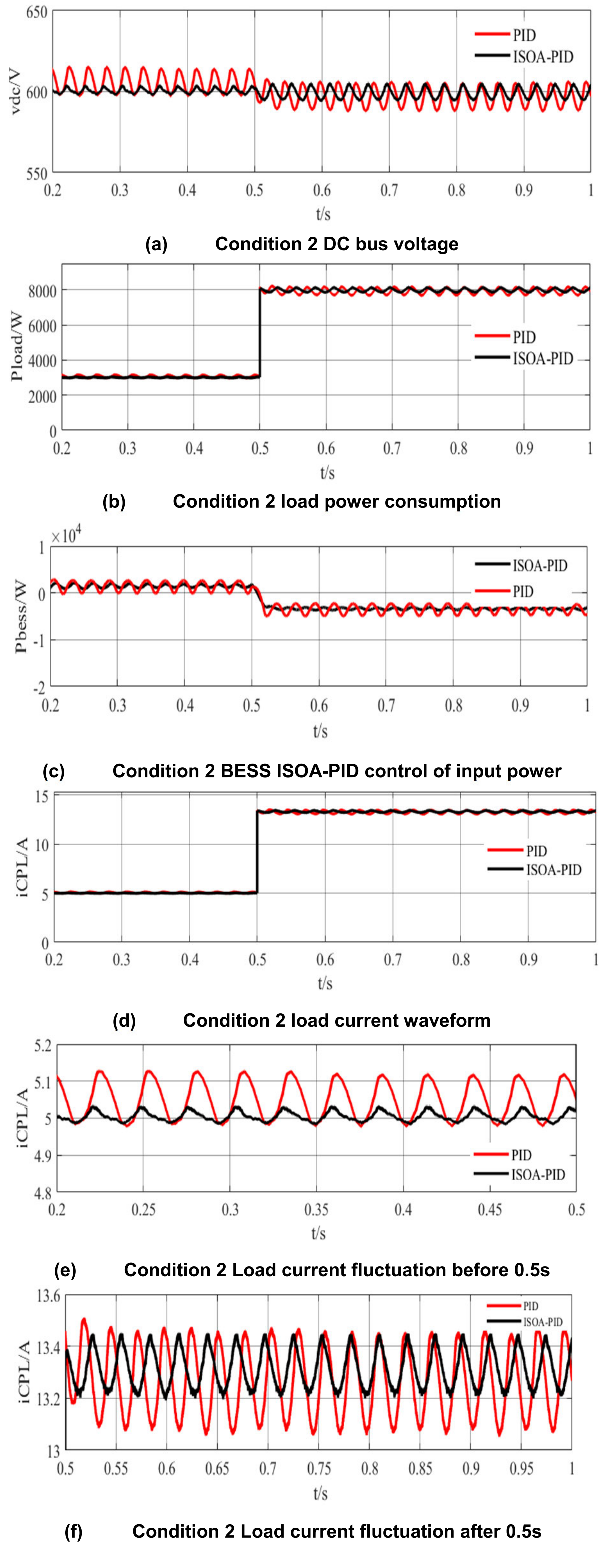

FIGURE 14. Output characteristics of microgrid under condition 2.

As shown in Fig.14(e), the PID-controlled load current i_{CPL} reaches highest fluctuation value $i_{CPL} = 5.14$A, and lowest fluctuation value $i_{CPL} = 4.97$A. ISOA-PID-controlled

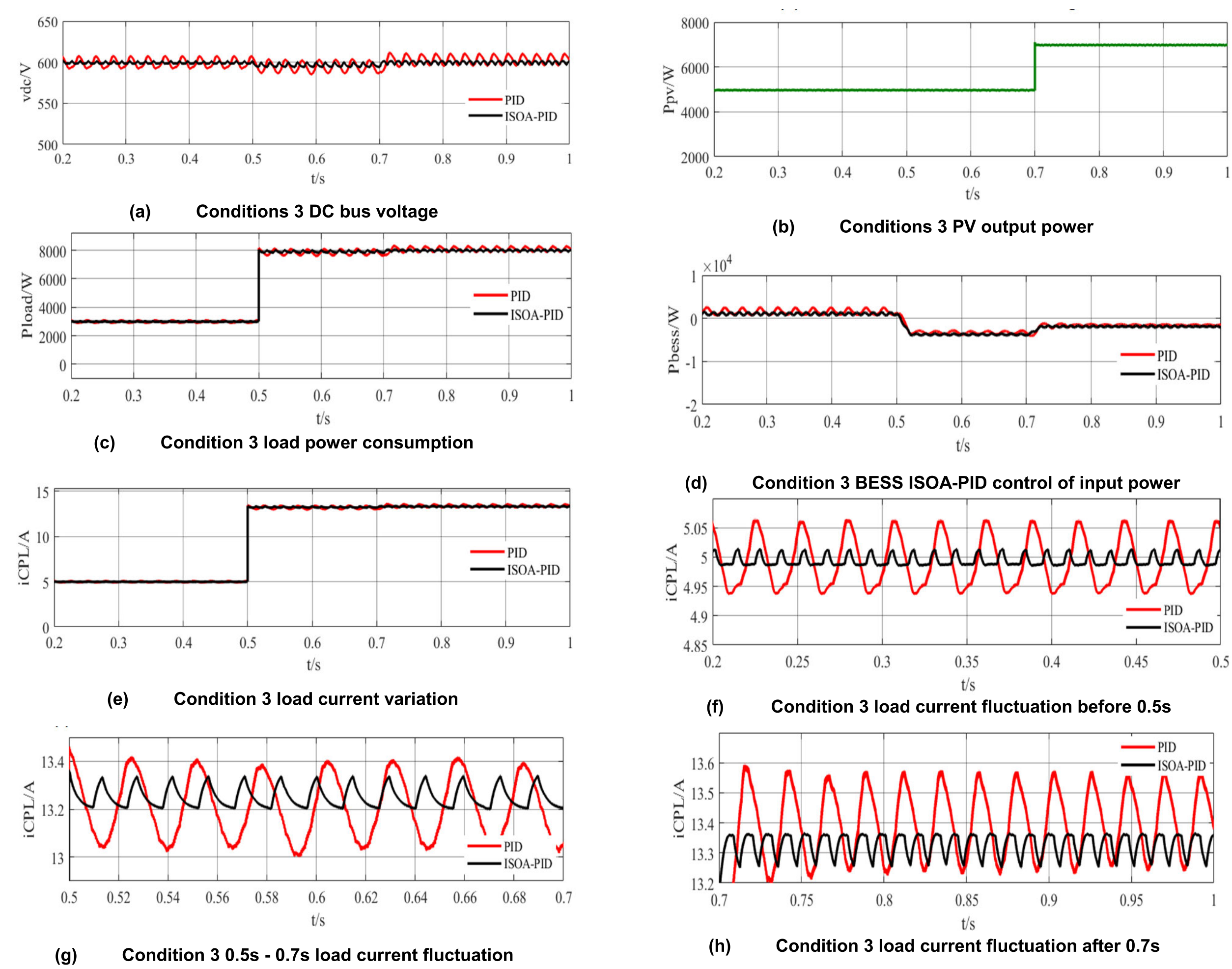

FIGURE 15. Output characteristics of microgrid under condition 3.

load current i_{CPL} reaches highest fluctuation value $i_{CPL} = 5.04$A, lowest fluctuation value $i_{CPL} = 4.98$A, and stable at about 5A, which is consistent with the theoretical simulation calculation results.

As shown in Fig.14(f), the PID-controlled load current i_{CPL} reaches highest fluctuation value $i_{CPL} = 13.51$A, and lowest fluctuation value $i_{CPL} = 13.10$A. ISOA-PID-controlled load current i_{CPL} reaches highest fluctuation value $i_{CPL} = 13.49$A, lowest fluctuation value $i_{CPL} = 13.20$A, and stable at around 13.33, which is consistent with the theoretical simulation calculation results.

The simulation results for working condition 2 are shown in Table 4. The data analysis shows that the proposed ISOA-PID control method has superior performance than the traditional PID control method in terms of suppressing the bus voltage oscillation and load current fluctuation under conditions of constant sunlight intensity and changing load demand.

3) CONDITION 3: BOTH SUNLIGHT INTENSITY AND LOAD POWER VARY.

The condition is set to sunlight intensity and the load demand changed. It requires the DC-DC converter of the PV system and the bi-directional DC-DC converter of the BESS to charge and discharge to jointly adjust the power to meet the load demand.

At the initial moment of the simulation, the load consumption is constant at $P_{CPL} = 3$kW and after 0.5s the load consumption is constant at $P_{CPL} = 8$kW. According to Ohm's law, the load current $i_{CPL} = 5$A before 0.5s and $i_{CPL} = 13.33$A after 0.5s. After 0.7s the sunlight intensity becomes greater, rising from 1000W/m^2 to 1500W/m^2.

TABLE 4. Stability performance of two control methods under condition 2.

Time	Control method	bus voltage			Load current
		Highest oscillation value	Lowest oscillation value	ripple percentage ((*Vmax–Vmin)/Vavg*)	ripple percentage ((*Imax–Imin)/Iavg*)
0.2s - 0.5s	PID	619V	599V	3.3%	3.4%
	ISOA-PID	602V	599V	0.5%	1.2%
>0.5s	PID	604V	583V	3.5%	3.1%
	ISOA-PID	604V	595V	1.5%	2.0%

Fig.15(a)-(h) show the simulated waveforms of DC bus voltage, PV system output power, load power consumption, BESS input power, and load current, respectively.

As shown in Fig.15(a), the bus voltage of the DC microgrid is stable. The PID-controlled bus voltage oscillation fluctuates greatly, with the highest oscillation value being 605V and the lowest oscillation value being 595V between 0.2s-0.5s. The highest oscillation value is 601V and the lowest oscillation value is 590V between 0.5s-0.7s. The highest oscillation value is 616V and the lowest oscillation value is 598V after 0.7s. While the ISOA-PID-controlled bus voltage oscillates at a maximum of 601V and a minimum of 599V between 0.2s-0.5s. The highest oscillation value is 600V and the lowest oscillation value is 596V between 0.5s-0.7s. The highest oscillation value is 601V and the lowest oscillation value is 598V after 0.7s.

As shown in Fig.15(b), the PV system reaches the steady state at 0.2s and the maximum output power is maintained at around 5kW until 0.5s, i.e., $P_{pv} = 5$kW. After 0.7s it is maintained at around 7kW, i.e., $P_{pv} = 7$kW. The dynamic transition process is smooth and rapid. The output power of the entire PV system is not affected by the DC microgrid, but only by the sunlight intensity and temperature.

As shown in Fig.15(c), the load power reaches the steady state at 0.2s, with constant $P_{CPL} = 3$kW before 0.5s and constant $P_{CPL} = 8$kW after 0.5s. i.e., $P_{load} = 3$kW before 0.5s and maintains $P_{load} = 8$kW after 0.5s.

As shown in Fig.15(d), the BESS is in a bi-directional flow state to maintain the bus voltage and compensate for or absorb the lack of load power from the PV system. The BESS reaches the steady state at 0.2s and is charging before 0.5s with power maintained at around 2kW, $P_{bess} = -2$kW. After 0.5s it is discharging, where the output power is maintained from 0.5s to 0.7s at around $P_{bess} = 3$kW, and after 0.7s the output power is maintained at around 1kW, $P_{bess} = 1$kW. The load power consumption is equal to the sum of the PV output power and the power provided by the BESS, according to equation (1), i.e., the net grid power $P_{net} = 0$W. The bus voltage is stable, and the expected results are obtained. In addition, the transition process at the 0.5s and 0.7s moments is smooth and fast.

As shown in Fig.15(e), after the load current reaches the steady state at 0.2s, the load current i_{CPL} is 5A before 0.5s and the load current i_{CPL} is 13.3A after 0.5s. The ISOA-PID control is more stable, and the load current fluctuates less than the PID control.

As shown in Fig.15(f), the PID-controlled load current i_{CPL} highest fluctuation value $i_{CPL} = 5.06$A, and the lowest fluctuation value $i_{CPL} = 4.94$A. The ISOA-PID-controlled load current i_{CPL} highest fluctuation value $i_{CPL} = 5.02$A and the lowest fluctuation value $i_{CPL} = 4.98$A, which is stabilized at around 5A.

As shown in Fig.15(g), the PID-controlled load current i_{CPL} has a maximum fluctuation value of $i_{CPL} = 13.41$A and a minimum fluctuation value of $i_{CPL} = 13.12$A. The ISOA-PID-controlled load current i_{CPL} has a maximum fluctuation value of $i_{CPL} = 13.31$A and a minimum fluctuation value of $i_{CPL} = 13.20$A, which is stabilized at around 13.33A.

TABLE 5. Stability performance of two control methods under condition 3.

Time	Control method	bus voltage			Load current
		Highest oscillation value	Lowest oscillation value	ripple percentage ((*Vmax*–*Vmin*)/*Vavg*)	ripple percentage ((*Imax*–*Imin*)/*Iavg*)
0.2-0.5s	PID	605V	595V	1.7%	2.4%
	ISOA-PID	601V	599V	0.3%	0.8%
0.5-0.7s	PID	601V	590V	1.8%	2.2%
	ISOA-PID	600V	596V	0.6%	0.8%
> 0.7s	PID	616V	598V	3.0%	2.9%
	ISOA-PID	601V	598V	1.0%	0.7%

As shown in Fig.15(h), the PID-controlled load current i_{CPL} has the highest fluctuation value $i_{CPL} = 13.59$A and the lowest fluctuation value $i_{CPL} = 13.21$A. The ISOA-PID-controlled load current i_{CPL} has the highest fluctuation value $i_{CPL} = 13.35$A and the lowest fluctuation value $i_{CPL} = 13.26$A, which is stable at around 13.33A. The above simulation results follow the theoretical calculation results.

The data from these simulations are shown in Table 5. The analysis of the data shows that the proposed ISOA-PID control method is superior to that of conventional PID control method in stabilizing bus voltage oscillations and load current fluctuations under the conditions of simultaneous changes in sunlight intensity and load power.

V. CONCLUSION

Robust and stable control of bus voltage in DC microgrid is the key issue to ensuring the reliability of the power supply. This paper analyses the structure principle and bus voltage regulation control of the photovoltaic-battery DC microgrid. An improved exponential variable step perturbation and observation method is proposed to control its maximum power output, and an ISOA-PID control method is proposed for the bus voltage regulation and control demand of BESS.

According to the simulation analyses, the exponential variable step perturbation and observation method has improved the response speed from 70ms to 10ms compared with the traditional perturbation and observation method. The amplitude of the output power fluctuation is reduced from 0.5W to 0.013W, thus it can be concluded that the proposed exponential variable step perturbation and observation method has the advantages of smaller energy loss, higher stability, and faster response.

The stability performance of the voltage and current under conventional PID control and ISOA-PID control are also compared through simulation analyses with three different operating conditions. The average ripple percentage of its voltage and current decreases from 3% to 1%. It concludes that ISOA-PID control can stabilize bus voltage oscillations and suppress load current fluctuations more effectively.

In the future work, more advanced MPPT algorithm under partial shading condition will be studied to improve the power generation efficiency of PV. Also, the hardware experimental platform will be built for more detailed experimental research.

REFERENCES

[1] Q. Xu, N. Vafamand, L. Chen, T. Dragicevic, L. Xie, and F. Blaabjerg, "Review on advanced control technologies for bidirectional DC/DC converters in DC microgrids," *IEEE J. Emerg. Sel. Topics Power Electron.*, vol. 9, no. 2, pp. 1205–1221, Apr. 2021, doi: 10.1109/JESTPE.2020.2978064.

[2] B. Aluisio, M. Dicorato, I. Ferrini, G. Forte, R. Sbrizzai, and M. Trovato, "Planning and reliability of DC microgrid configurations for electric vehicle supply infrastructure," *Int. J. Electr. Power Energy Syst.*, vol. 131, Oct. 2021, Art. no. 107104, doi: 10.1016/j.ijepes.2021.107104.

[3] A. Chandra, G. K. Singh, and V. Pant, "Protection techniques for DC microgrid–A review," *Electr. Power Syst. Res.*, vol. 187, Oct. 2020, Art. no. 106439, doi: 10.1016/J.EPSR.2020.106439.

[4] F. S. Al-Ismail, "DC microgrid planning, operation, and control: A comprehensive review," *IEEE Access*, vol. 9, pp. 36154–36172, 2021, doi: 10.1109/ACCESS.2021.3062840.

[5] Y. Mi, J. Guo, S. Yu, P. Cai, L. Ji, Y. Wang, D. Yue, Y. Fu, and C. Jin, "A power sharing strategy for islanded DC microgrid with unmatched line impedance and local load," *Electr. Power Syst. Res.*, vol. 192, Mar. 2021, Art. no. 106983, doi: 10.1016/j.epsr.2020.106983.

[6] M. Mehdi, S. Z. Jamali, M. O. Khan, S. Baloch, and C.-H. Kim, "Robust control of a DC microgrid under parametric uncertainty and disturbances," *Electr. Power Syst. Res.*, vol. 179, Feb. 2020, Art. no. 106074, doi: 10.1016/j.epsr.2019.106074.

[7] M. Sechilariu, B. C. Wang, F. Locment, and A. Jouglet, "DC microgrid power flow optimization by multi-layer supervision control. Design and experimental validation," *Energy Convers. Manag.*, vol. 82, pp. 1–10, Jun. 2014, doi: 10.1016/j.enconman.2014.03.010.

[8] Y. Zheng, Y. Song, A. Huang, and D. J. Hill, "Hierarchical optimal allocation of battery energy storage systems for multiple services in distribution systems," *IEEE Trans. Sustain. Energy*, vol. 11, no. 3, pp. 1911–1921, Jul. 2020, doi: 10.1109/TSTE.2019.2946371.

[9] H. Kakigano, Y. Miura, and T. Ise, "Distribution voltage control for DC microgrids using fuzzy control and gain-scheduling technique," *IEEE Trans. Power Electron.*, vol. 28, no. 5, pp. 2246–2258, May 2013, doi: 10.1109/TPEL.2012.2217353.

[10] G. Bruni, S. Cordiner, V. Mulone, V. Rocco, and F. Spagnolo, "A study on the energy management in domestic micro-grids based on model predictive control strategies," *Energy Convers. Manage.*, vol. 102, pp. 50–58, Sep. 2015, doi: 10.1016/j.enconman.2015.01.067.

[11] D. Tengfei, M. Jingfeng, D. Yinjia, Y. Chunyun, and Z. Xiaotong, "Bus voltage stability control of the distributed photovoltaic and energy storage DC microgrid based on ADRC," in *Proc. IEEE Int. Conf. Recent Adv. Syst. Sci. Eng. (RASSE)*, Dec. 2021, pp. 1–7, doi: 10.1109/RASSE53195.2021.9686941.

[12] J. Sun, W. Lin, M. Hong, and K. A. Loparo, "Voltage regulation of DC-microgrid with PV and battery," *IEEE Trans. Smart Grid*, vol. 11, no. 6, pp. 4662–4675, Nov. 2020, doi: 10.1109/TSG.2020.3005415.

[13] R. K. Chauhan, K. Chauhan, and J. M. Guerrero, "Controller design and stability analysis of grid connected DC microgrid," *J. Renew. Sustain. Energy*, vol. 10, no. 3, May 2018, Art. no. 035101, doi: 10.1063/1.5024714.

[14] H. Doubabi, I. Salhi, and N. Essounbouli, "A novel control technique for voltage balancing in bipolar DC microgrids," *Energies*, vol. 15, no. 9, p. 3368, May 2022, doi: 10.3390/en15093368.

[15] B. Xiaojuan, Z. Wujun, and F. Jinglu, "Application of PID control algorithm based on genetic BP network for mold-free drawing temperature control," *J. Univ. Sci. Technol. Beijing*, vol. 30, no. 12, pp. 1439–1442, 2008, doi: 10.13374/j.issn1001-053x.2008.12.013.

[16] Y. Kang, Z. Li, and T. Wang, "Application of PID control and improved ant colony algorithm in path planning of substation inspection robot," *Math. Problems Eng.*, vol. 2022, pp. 1–10, Aug. 2022, doi: 10.1155/2022/9453219.

[17] Y. Liu, D. Jiang, and J. Yun, "Self-tuning control of manipulator positioning based on fuzzy PID and PSO algorithm," *Frontiers Bioeng. Biotechnol.*, vol. 18, no. 9, pp. 1385–1396, 2022, doi: 0.3389/fbioe.2021.817723.

[18] M. Tuba, I. Brajevic, and R. Jovanovic, "Hybrid seeker optimization algorithm for global optimization," *Appl. Math. Inf. Sci.*, vol. 7, no. 3, pp. 867–875, May 2013.

[19] A. R. Jordehi, "Seeker optimisation (human group optimisation) algorithm with chaos," *J. Experim. Theor. Artif. Intell.*, vol. 27, no. 6, pp. 753–762, Nov. 2015, doi: 10.1080/0952813x.2015.1020568.

[20] B. Babaiahgari, M. H. Ullah, and J.-D. Park, "Coordinated control and dynamic optimization in DC microgrid systems," *Int. J. Electr. Power Energy Syst.*, vol. 113, pp. 832–841, Dec. 2019, doi: 10.1016/j.ijepes.2019.05.076.

[21] T. Alnejaili, S. Drid, D. Mehdi, L. Chrifi-Alaoui, R. Belarbi, and A. Hamdouni, "Dynamic control and advanced load management of a stand-alone hybrid renewable power system for remote housing," *Energy Convers. Manage.*, vol. 105, pp. 377–392, Nov. 2015, doi: 10.1016/j.enconman.2015.07.080.

[22] T. Dragicevic, J. M. Guerrero, J. C. Vasquez, and D. Škrlec, "Supervisory control of an adaptive-droop regulated DC microgrid with battery management capability," *IEEE Trans. Power Electron.*, vol. 29, no. 2, pp. 695–706, Feb. 2014, doi: 10.1109/TPEL.2013.2257857.

[23] M. D. and V. Sankaranarayanan, "A novel nonlinear sliding mode controller for a single stage grid-connected photovoltaic system," *ISA Trans.*, vol. 107, pp. 329–339, Dec. 2020, doi: 10.1016/j.isatra.2020.07.021.

[24] A. Charaabi, A. Zaidi, O. Barambones, and N. Zanzouri, "Implementation of adjustable variable step based backstepping control for the PV power plant," *Int. J. Electr. Power Energy Syst.*, vol. 136, Mar. 2022, Art. no. 107682, doi: 10.1016/j.ijepes.2021.107682.

[25] A. Harrag and S. Messalti, "Variable step size modified P&O MPPT algorithm using GA-based hybrid offline/online PID controller," *Renew. Sustain. Energy Rev.*, vol. 49, pp. 1247–1260, Sep. 2015, doi: 10.1016/j.rser.2015.05.003.

[26] B. Li, L. Zhang, and Y. Zichun, "Reconstruction of Dykas turbine blade grille profiles based on crowd search algorithm," *Propuls. Technol.*, vol. 41, no. 11, pp. 2530–2537,2020, doi: 10.13675/j.cnki.tjjs.200384.

[27] Z. Zhu, Y. Liu, Y. He, W. Wu, H. Wang, C. Huang, and B. Ye, "Fuzzy PID control of the three-degree-of-freedom parallel mechanism based on genetic algorithm," *Appl. Sci.*, vol. 12, no. 21, p. 11128, Nov. 2022, doi: 10.3390/app122111128.

[28] K. R. M. Vijaya Chandrakala, S. Balamurugan, and K. Sankaranarayanan, "Variable structure fuzzy gain scheduling based load frequency controller for multi source multi area hydro thermal system," *Int. J. Electr. Power Energy Syst.*, vol. 53, pp. 375–381, Dec. 2013, doi: 10.1016/j.ijepes.2013.05.009.

[29] X.-J. Wu, L. Xu, R. Zhen, and X.-L. Wu, "Global and local moth-flame optimization algorithm for UAV formation path planning under multi-constraints," *Int. J. Control, Autom. Syst.*, vol. 21, no. 3, pp. 1032–1047, Mar. 2023, doi: 10.1007/s12555-020-0979-3.

[30] B. Khokhar, S. Dahiya, and K. P. S. Parmar, "Load frequency control of a microgrid employing a 2D sine logistic map based chaotic sine cosine algorithm," *Appl. Soft Comput.*, vol. 109, Sep. 2021, Art. no. 107564, doi: 10.1016/j.asoc.2021.107564.

[31] W. Xinzhong, H. Zhenghua, W. Lianjiang, Z. Yuxiao, X. Jialin, and L. Ang, "Intelligent on-demand regulation algorithm and key technology for mine wind flow," *J. China Univ. Mining Technol.*, vol. 50, no. 4, pp. 725–734, 2021, doi: 10.13247/j.cnki.jcumt.001316.

[32] A. Korompili and A. Monti, "Review of modern control technologies for voltage regulation in DC/DC converters of DC microgrids," *Energies*, vol. 16, no. 12, p. 4563, Jun. 2023, doi: 10.3390/en16124563.

AIHUA WU received the B.E. degree in industrial automation from Nantong University, China, in 2000, the M.Sc. degree in electrical engineering from Nanjing University of Aeronautics and Astronautics, China, in 2006, and the Ph.D. degree in electrical engineering from Jiangsu University, China, in 2019. She is currently an Associate Professor with the School of Mechanical Engineering, Nantong University. Her current research interests include electrical machines and drives, and renewable energy generation and applications.

RUI GONG received the B.E. degree in electrical engineering and intelligent control from East China Jiaotong University, Nanchang, China, in 2019. He is currently pursuing the M.Sc. degree with Nantong University. His current research interests include renewable energy generation and automatic generation control.

JINGFENG MAO received the B.E. degree in industrial automation from Wuhan University of Technology, Wuhan, China, in 1998, and the M.Sc. and Ph.D. degrees in electrical engineering from Jiangsu University, Zhenjiang, China, in 2004 and 2008, respectively. He is currently a Professor with the School of Electrical Engineering, Nantong University. His current research interests include electrical machines and drives, renewable energy generation and applications, and control of microgrids.

XIUYONG YU received the B.E. degree in electrical engineering from China Agricultural University (CAU), China, in 2015, and the Ph.D. degree from the Institute of Electrical Engineering, Chinese Academy of Sciences, China, in 2021. He is currently a Lecturer with the School of Electrical Engineering, Nantong University. His main research interests include fault protection of dc distribution networks and MMC-HVdc grids, and renewable energy.

JIANJUN HE received the B.E. degree in industrial automation from Wuhan University of Technology, China, in 1996. He is currently pursuing the M.Sc. degree with Nantong University. He is a Senior Engineer with Jiangsu Hantong Group. His main research interests include offshore wind power generation and distribution network control.

E'XIANG LI received the B.E. degree in electrical engineering and automation from Yangzhou University, China, in 2005. He is currently pursuing the M.Sc. degree with Nantong University. He is an Engineer with Jiangsu Hantong Group. His main research interests include offshore wind power generation and ship power systems.